frontiers | Frontiers in Earth Science

TYPE Original Research
PUBLISHED 21 April 2023
DOI 10.3389/feart.2023.1080472

OPEN ACCESS

EDITED BY
Xiaoping Zhou,
Chongqing University, China

REVIEWED BY
Xiangchao Shi,
Southwest Petroleum University, China
Chinedu J. Okere,
Texas Tech University, United States

*CORRESPONDENCE
Dongming Zhang,
zhangdongming@jxust.edu.cn

SPECIALTY SECTION
This article was submitted to Geohazards and Georisks,
a section of the journal
Frontiers in Earth Science

RECEIVED 26 October 2022
ACCEPTED 20 March 2023
PUBLISHED 21 April 2023

CITATION
Geng J, Liu J, Zeng G, Zhang D, Guo Z and Xu J (2023), Experimental study on the evolution characteristics of gas pressure field for true triaxial cyclic mining.
Front. Earth Sci. 11:1080472.
doi: 10.3389/feart.2023.1080472

Experimental study on the evolution characteristics of gas pressure field for true triaxial cyclic mining

Jiabo Geng[1,2,3,4], Jiangtong Liu[1], Gaoxiong Zeng[1], Dongming Zhang[1,5]*, Zhigguo Guo[1] and Jiang Xu[5]

[1]School of Emergency Management and Safety Engineering, Jiangxi University of Science and Technology, Ganzhou, China, [2]Sinosteel Maanshan General Institute of Mining Research Co. Ltd, Maanshan, Anhui, China, [3]Ganzhou Key Laboratory of Industrial Safety and Emergency Technology, Ganzhou, China, [4]Center for Emergency Management and Multidisciplinary Innovation Research, Jiangxi University of Science and Technology, Ganzhou, China, [5]State Key Laboratory of Coal Mine Disaster Dynamics and Control, Chongqing University, Chongqing, China

The evolution characteristics of coal seam strain and gas pressure in circular mining were explored by conducting physical simulation tests on the influence of cyclic stress on coal seam parameters under different initial gas pressures using a large true triaxial physical simulation test rig. The evolution characteristics of gas pressure and coal seam strain with the number of cycles and gas pressure were discussed. The test results showed that during cyclic loading and unloading, the coal seam is cracked under stress and new cracks are generated, and the new fractures cause the overall pressure of the coal seam methane to decrease by adsorbing more free gas. In the loading stage, the coal skeleton is squeezed by stress, which causes the space of coal seam pores and cracks to shrink, the free gas in the pores and fractures of the coal seam is extruded, and the strain and gas pressure of the coal seam increase with the increase of stress. In the unloading stage, the reduction of stress leads to the coal skeleton tending to return to its initial state, the free gas in the pores is transported and enriched into the fractures of the coal seam, and the strain and gas pressure of the coal seam are gradually reduced. With the increase of the number of cycles, the damage of the coal seam increases and deformation occurs, the increasing amplitude of gas pressure gradually increases during loading, and the decreasing amplitude of gas pressure gradually decreases when unloading, and the closer the distance from the pressurized boundary, the greater the amplitude change. Under different initial gas pressure conditions, the greater the initial gas pressure, the greater the increasing amplitude of gas pressure and the smaller the decreasing amplitude.

KEYWORDS

cyclic loading and unloading, initial gas pressure, strain, change in gas pressure, coal permeability field

1 Introduction

With the advent of the era of deep coal mining in China, as the largest deep coal mining country, China's coal industry has long been threatened by deep mining and gas dynamic disasters. Therefore, the prevention and control of coal and gas dynamic disasters has become an urgent problem to be solved in the field of coal mining (Lin et al., 2015; Li et al.,

2021). The dynamic disasters of coal and gas in deep mining of coal mine are mainly characterized by three kinds of disaster modes: rock burst, coal and gas outburst and their composite (Pan, 2016). The study found that coal and gas dynamic disasters are often accompanied by coal and gas outburst. Scholars have done a lot of research on coal and gas outburst (Geng et al., 2017; Nie et al., 2022a; Wang et al., 2022a; Nie et al., 2022b; Wang et al., 2022b). The results show that the outburst occurs under the combined action of three main factors: the physical and mechanical properties of coal, gas pressure and ground stress (Zhou and He, 1990; Wang et al., 2018a; Gao et al., 2019; Lu et al., 2020). In the incubation stage of outburst, the migration of gas in coal seam is mainly affected by mining stress. When deep mining is carried out in coal seam, the redistribution of ground stress in mining face will cause the redistribution of gas (Yan et al., 2015; Xu et al., 2018). In view of the distribution characteristics of stress in mining face, many scholars have carried out similar simulation experiments (He et al., 2021; Zhang et al., 2021; Liu et al., 2022; Tao et al., 2022; Yao et al., 2022), mainly through the simulation of loading mode and load size (Wang et al., 2020; Cheng et al., 2021; Ren et al., 2021) to study the influence of coal damage on coal permeability characteristics. For example, Sun et al. (2016) made an experimental device to study the relationship between permeability and axial stress of coal samples through axial loading and unloading. Compared with uniaxial loading, triaxial loading test is more practical (Hu et al., 2016; Yang et al., 2019). Zhao et al. (2020a) used electro-hydraulic servo rock mechanics test system (MTS 15) to carry out conventional triaxial and cyclic loading-unloading tests on granite under different circumferential pressures, and obtained the corresponding stress-strain curves and deformation damage characteristics. Zou et al. (2016) carried out uniaxial and triaxial mechanical strength tests on raw coal samples under conventional and cyclic loading, and systematically studied the damage evolution law of raw coal under uniaxial and triaxial cyclic loading by using acoustic emission technology (Zhang et al., 2020). Through the above research on the damage evolution law and deformation and failure characteristics of coal seam, it is helpful for later researchers to analyze the seepage characteristics of coal body (Xu et al., 2014; Chen et al., 2018; Zhao et al., 2020b). For the study of coal seepage, scholars are more inclined to study the loading path. For example, Li et al. (2019) mentioned three different cyclic loading and unloading paths, namely, step-by-step cyclic path, step-by-step incremental cyclic path and cross-cycle path, in order to obtain the phenomenon that the permeability of coal samples increases after the stress exceeds the yield stage during the loading process.

In summary, scholars have done a lot of research on uniaxial and triaxial cyclic loading and unloading of coal under different conditions to study its permeability characteristics and stress, strain and damage of coal under stress (Wang et al., 2018b; Jia et al., 2018). However, there are relatively few studies on the change of gas pressure, migration characteristics and physical field evolution characteristics in coal under large-scale true triaxial cyclic loading and unloading (Duo et al., 2018; Liu et al., 2020). In view of this, this experiment simulates the influence of cyclic disturbance on gas pressure change, migration characteristics and internal damage of coal body in the process of coal mining through large-scale true triaxial test equipment, and provides reference materials for preventing coal and gas dynamic disasters in actual mining.

2 Experimental equipment and scheme

2.1 Laboratory equipment

The experimental equipment is an independently developed physical simulation test system for coal and gas dynamic disasters (Liu et al., 2013a), and the equipment has the characteristics of large size, large applied pressure, and many built-in and external sensors compared with previous equipment. The loading equipment is individually controlled by nine sets of independent servo-controlled loading systems. The equipment is 1 m long, 0.41 m wide and high, and the applied pressure range is 0–80 MPa. Multiple pressure sensors are arranged in the equipment, which can collect the gas pressure changes of each coal seam more accurately, and external displacement sensor at the equipment indenter for effective collection of coal data. It can physically simulate gas desorption, adsorption, pressure change, and enrichment processes under different conditions. As shown in Figure 1, Figure 1A shows the physical graph, and Figure 1B shows the relationship diagram of several factors.

2.2 Experimental coal sample

(1) Production of coal sample: The coal samples were collected from a coal mine in Jiangxi Province. Figure 2 shows the geographical location of the coal mine. About 2 tons of raw coal were obtained under the mine, and the coal was crushed, and the coal powder with different particle sizes was sieved and stored by the sieving machine. The coal samples were finally put into the specimen box and pressed into the coal specimen by using the coal specimen pressure forming machine.

(2) Arrangement of sensors: While placing the raw coal into the specimen box, the gas pressure sensor is arranged at the set position of the box. As shown in Figure 3. The gas pressure sensor is numbered according to different positions. The pressure sensor at the center of the first section (z = 919 mm) is labeled as P1, and then the number value is increased clockwise. The sensor in the first section is numbered as P1 ~ P9, and the sensor in the second section (z = 657 mm) is numbered as P10 ~ P18.

(3) vacuum pumping: One end of the gas pipe is connected with a box inflation hole, and the other end is connected with a vacuum pump for vacuum pumping. The pressure value of the gas pressure sensor in the observation box can be reduced to −0.1 MPa.

(4) Loading and inflating: A total of 9 pressure heads in 3 directions of the box are loaded to the initial stress value of the experimental design, and the gas cylinder is opened after the loading pressure is completed. The gas required for the experiment is filled into the box to the set pressure value.

(5) Adsorb: After the gas is completed, the coal sample is fully adsorbed for 48 h, the gas pressure change in the box is observed, and the gas is inflated once every 0.5 h.

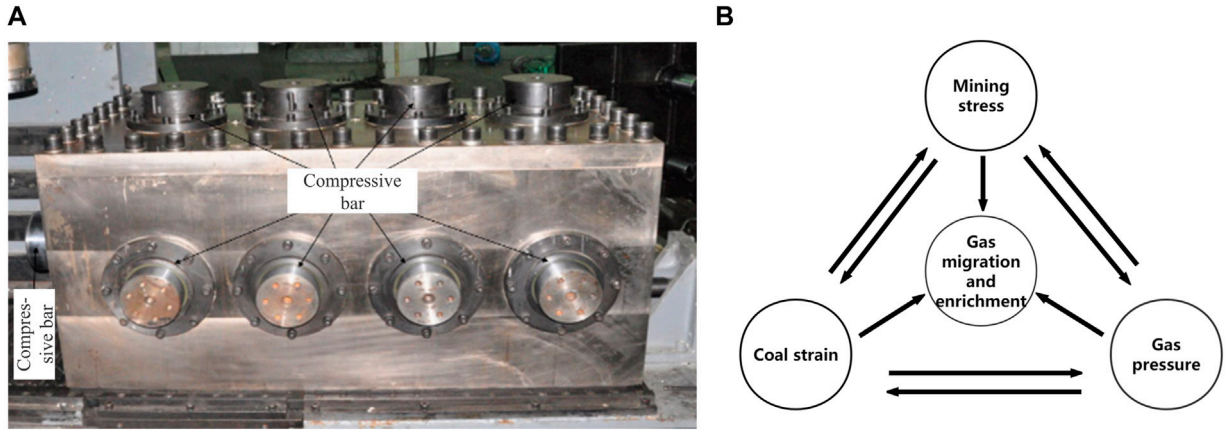

FIGURE 1
Multifield coupling test system for dynamic disasters in coal mines, **(A)** Real figure, **(B)** Relationship of factors.

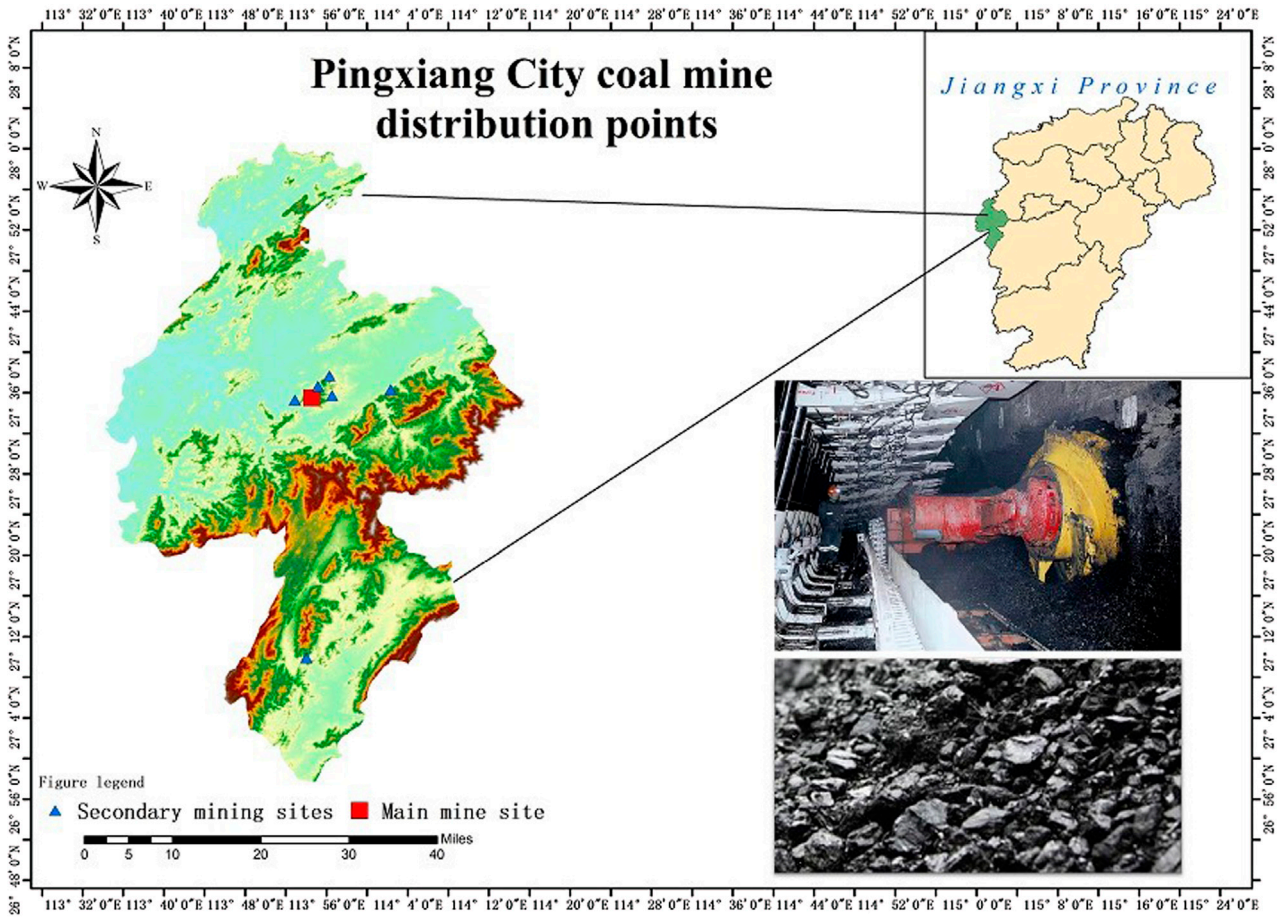

FIGURE 2
The geographic location map of the study area.

(6) Cyclic disturbance: After the coal sample fully absorbs the gas until the gas pressure in the box is stable, the loading and unloading stress of the nine indenters is controlled to simulate the cyclic disturbance test of the coal under uneven stress. Through the data collected by each sensor, the physical field changes of coal samples are analyzed.

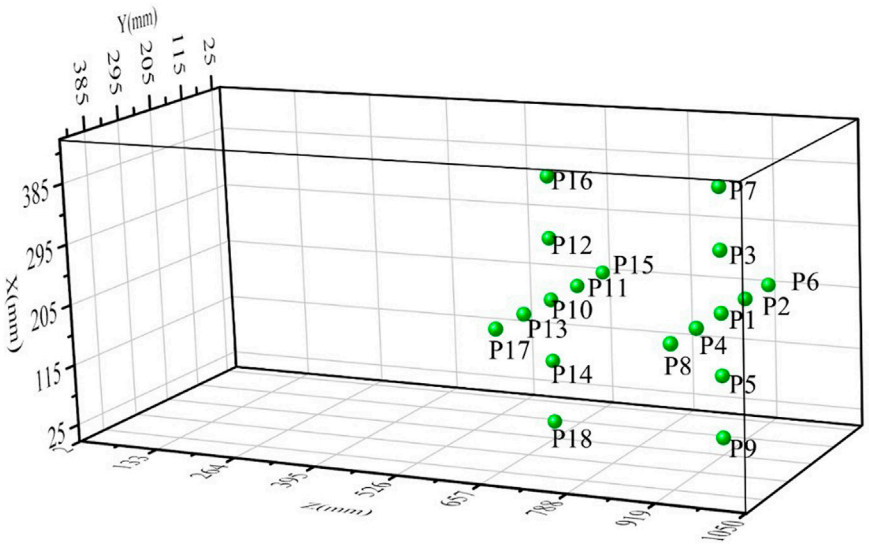

FIGURE 3
Schematic diagram of gas pressure sensor installation positions.

2.3 Experimental scheme

This paper refers to the stress distribution law (Xie et al., 2011) and conclusion in front of coal mining work under topping coal mining, takes the coal seam occurrence conditions of 1,000 m as the background, simulates the change of the stress in front of the mine mining work by simulating the main stress of true triaxial cyclic loading and unloading, explores the evolution characteristics of coal seam parameters and the law of coal seam gas migration under cyclic mining disturbance, and measures the distribution of air pressure in the box, and then summarizes the enrichment law of coal bed methane under circulating load.

According to the empirical formula of the change in crustal stress with buried depth in China (Li et al., 2012), the vertical stress of the coal seam can be written as follows:

$$\sigma_v = 0.0208H + 2.195 = 23\text{MPa}\,. \quad (1)$$

The test coal seam's maximum thickness is 4.80 m, and the density is 1,420 kg/m^3. The height of the box is 0.41 m, and the density of the briquette is 1,380 kg/m^3. The geometric similarity formula was used to obtain the geometric similarity ratio of approximately 11.5. The simulated stress σ is 2 MPa, and the gas pressure P is 1 MPa.

According to the stress distribution law in front of the working face, the four pressure heads above the box are set to provide the maximum principal stress, and they are named as σ11–σ14 and σ11 = (0.6–1) σ, σ12 = (0.9–1.5) σ, σ13 = (1.5–2.5) σ, and σ14 = (0.3–0.5) σ. An indenter at the rear of the container provides the intermediate principal stress (σ2 = (0.6–1) σ). The four pressure heads on the side of the container provide the minimum principal stress as σ31 = (0.35–0.6) σ, σ32 = (0.5–0.9) σ, σ33 = (0.9–1.5) σ, and σ34 = (0.175–0.3) σ. The hydraulic cylinder in the hydraulic servo loading system provides the loading and unloading stresses. The gas pressure sensor is embedded in the loading and unloading pressure heads and distributed in the three directions of the specimen box. The pressure of the coal seam in nine loading and unloading positions is measured. Each operation takes 10 min. Figure 4 shows the simulated box diagram. According to the distribution characteristics of the three stress zones, each pressure head's stress value is calculated as shown in Table 1.

3 Experimental testing and analysis

3.1 Evolution characteristics of gas pressure, coal strain and permeability under cyclic loading

The disturbance results in some changes in coal rock stress, gas pressure, and the physical and mechanical properties of the coal rock, causing gas migration, and distribution of gas migration is related to the risk of gas outbursts (Xie et al., 2011; Liu et al., 2013b). This section explores the relationship among disturbance stress, coal rock mass strain, and gas strain in coal rock by conducting 11 true triaxial cyclic load tests by simulating the disturbance of coal rock mining.

Figure 5A shows the P3 gas pressure change curve under 11 cycles of cyclic loading at an initial gas pressure of 1.007 MPa. It can be seen from the figure that as the number of cycles increases, the gas pressure decreases as a whole, and the gas pressure finally decreases from 1.007 MPa before loading to 0.998 MPa at the end of the cycle. This is because the effect of cyclic stress makes the cumulative damage of coal gradually increased, resulting in new cracks in coal and adsorption of more free gas molecules. During the whole cycle, the gas pressure increases with the increase of stress and decreases with the decrease of stress. The reason is that loading stress leads to coal skeleton compression, coal pore becomes smaller

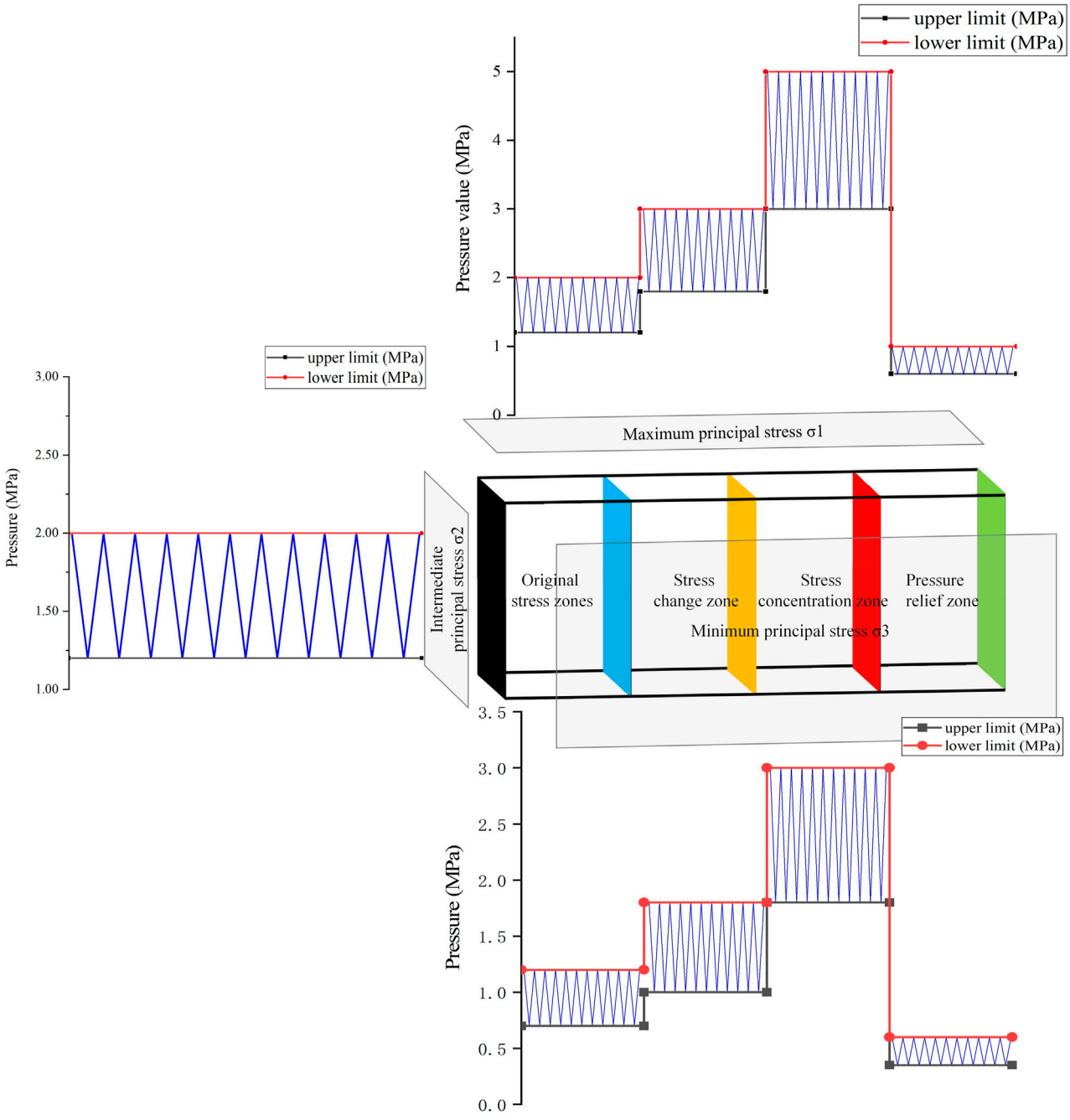

FIGURE 4
Simulated box and stress distribution diagram.

TABLE 1 Schemes of simulated cyclic mining disturbance stress test.

Test type	The stress parameter evolution scheme in the cyclic disturbed mining process is simulated									
The stress state (MPa)	Stress number	σ11	σ12	σ13	σ14	σ31	σ32	σ33	σ34	σ2
	Lower limit	1.2	1.8	3	0.6	0.7	1	1.8	0.35	1.2
	Ceiling	2	3	5	1	1.2	1.8	3	0.6	2
Loading and unloading rate (min/MPa)		0.08	0.12	0.2	0.04	0.05	0.08	0.12	0.025	0.08

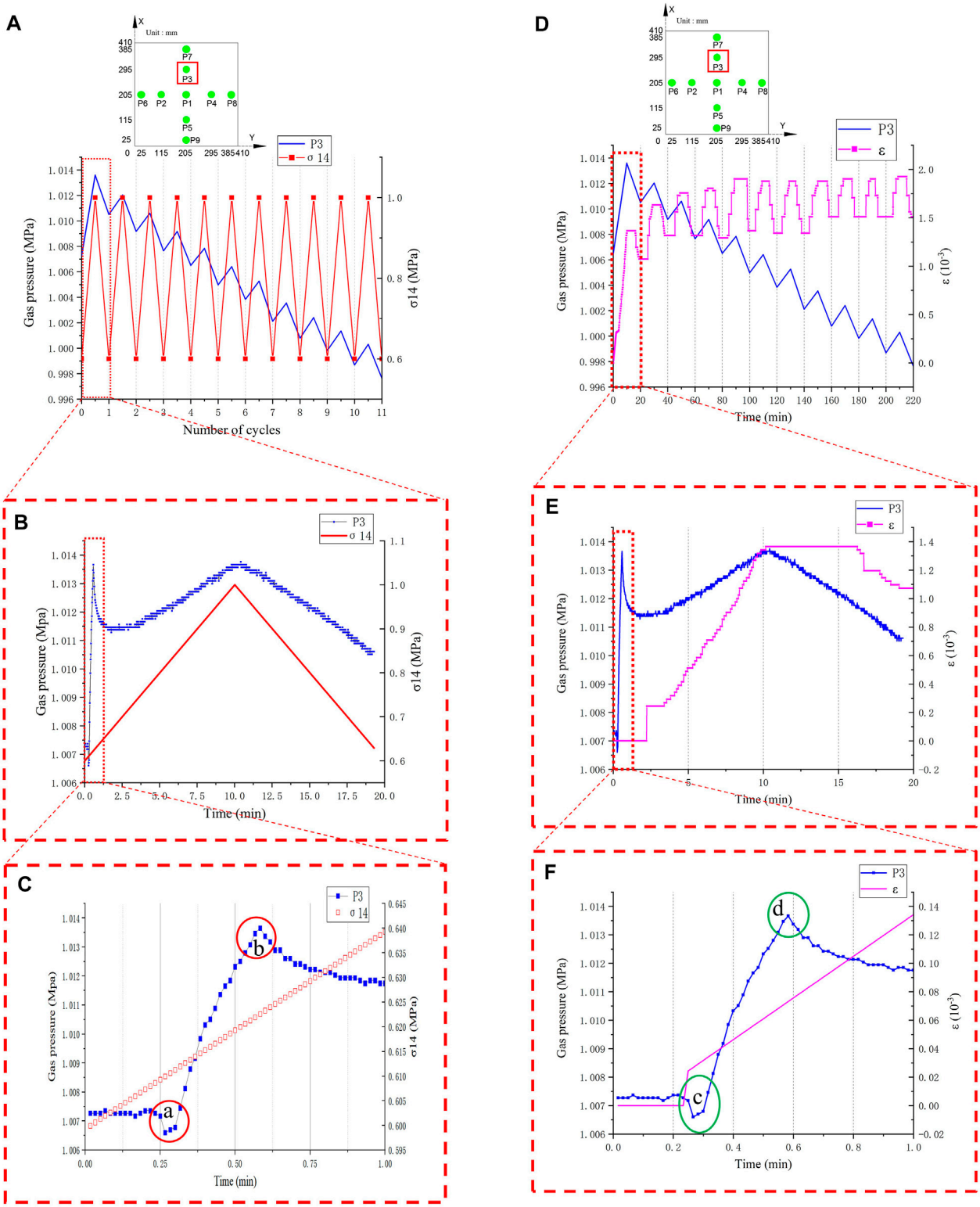

FIGURE 5
The variation of gas pressure with stress and strain. **(A)** The variation in gas pressure with stress under 11 cyclic loads. **(B)** The change in gas pressure with stress under the first cyclic load. **(C)** The change in gas pressure with stress under the previous minute loading. **(D)** The variation in gas pressure and coal strain under 11 cyclic loads. **(E)** The change in gas pressure and coal strain under the first cyclic load. **(F)** The change in gas pressure and coal strain under loading in the last minute.

and gas pressure increases. Unloading stress leads to compression recovery of coal skeleton, increase of coal pore and decrease of gas pressure.

After the first loading and unloading, the gas pressure value is higher than that before loading and unloading (Figure 5B). During the first loading and unloading stress, the gas pressure change analysis showed that 0.6 min before loading, the coal seam is squeezed, the pore space of the coal seam becomes smaller, resulting in a sharp rise in gas pressure. Subsequently, the gas molecules are diffused due to the thermal movement and are transferred to other positions in the coal through the matrix pore network, and the gas pressure at P3 gradually slows down to 1.015 MPa. The subsequent loading stress destructs the coal, and the amount of gas adsorbed by coal seam under the loading tends to balance with the amount of gas that the coal seam is squeezed. When the loading stress continues until the end, the gas that is squeezed out of the pores of the coal gradually increases, and the gas pressure reaches the maximum once again. The gas pressure decreases gradually due to gas adsorption by pores and new fissures in the unloading stage. At the end of the cycle, the gas pressure value is higher than that before the loading, indicating that plastic strain has occurred under the first loading and unloading, and the tiny pores in the coal seam are destroyed by compression. After unloading, the pores cannot return to the initial state, leading to a higher gas pressure than before the loading.

The gas drops briefly 1 minute before the first loading (Figure 5C). In the first 0.25 min, the stress increase does not reach the pressure condition for coal deformation, and the gas pressure value of coal remains unchanged. As the stress increases, the coal seam is compacted and slightly deformed (area a of Figure 5C). The gas pressure does not increase but suddenly decreases due to the gas diffusion phenomenon. Then, within 0.35 min of the loading stress, the coal seam deforms and gradually increases and a large number of gas molecules are desorbed in the pores of the coal seam. The gas pressure increases rapidly and reaches the maximum value of 1.01366 MPa, with a change of 6.39×10^{-3} MPa (area b in Figure 5C). In the last 0.4 min, the gas molecules diffuse from the high-pressure area to the low-pressure area and move from the P3 gas pressure sensor to the P9 gas pressure sensor in the general direction, gradually decreasing the gas pressure value at P3. As the stress increases, the gas pressure tends to 1.012 MPa and reaches a new dynamic equilibrium state. Each gas pressure sensor's data analysis showed that the gas pressure changes similarly under 11 loading and unloading cycles.

In the cyclic load test, the coal seam deforms. The relationship between gas pressure and strain is obtained through data analysis. Figure 5D shows the P3 gas pressure and coal strain curve on the longitudinal section line of the first section with the change in cyclic loading and unloading time. The strain and gas pressure gradually increase at the loading stage during the 11 cycles of loading and unloading. In the unloading stage, the strain and gas pressure decrease gradually. As loading and unloading continue, the coal strain becomes stable at approximately 1.5×10^{-3}. From the analysis, the coal seam damage degree gradually increases in the first 80 min of cyclic loading and unloading stress, whereas its strain variable does not reach the maximum value. When it reaches 90 min, the coal seam damage degree reaches the maximum value, close to 2×10^{-3}. The strain upper limit is almost unchanged in each subsequent loading stage, close to 2×10^{-3}. At the unloading stage of

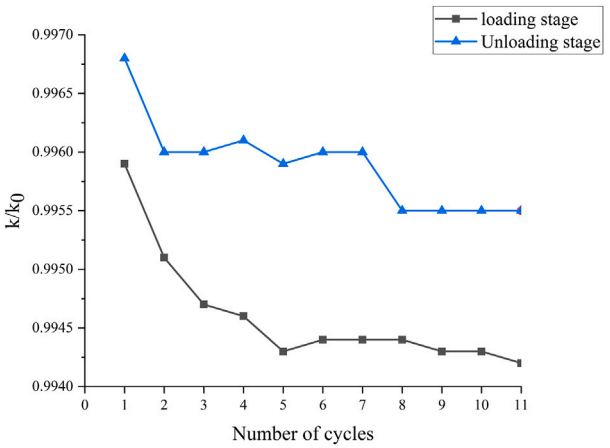

FIGURE 6
Relationship between permeability ratio and cycle times.

140–220 min, the lower limit of coal strain is almost unchanged, which is close to 1.5×10^{-3}. The strain at the end of the last four unloadings is larger than that at the end of the first seven unloadings, indicating that under the stress of the last four unloadings, the damage degree of coal seam is more severe at the end of the first 7 unloading and the deformation repairability of coal at the end of the last 4 unloading is worse than that at the end of the first 7 unloading. During the unloading phase in the first cycle, the strain is approximately 1.35×10^{-3}, which is the minimum strain in 11 loads, and at the end of the 20-min unloading, the strain was approximately 1.10×10^{-3}, which is the minimum strain in 11 loads. Therefore, the damage degree of coal seam is the minimum and its repairability after deformation is the best. As shown in Figure 6.

Figure 5E shows the curve of gas pressure and coal strain changes under loading and unloading stress in the first 20 min. From the analysis, it is observed that 2.5 min before loading, the coal strain increases directly with the stress due to the small coal deformation and the elasticity of the coal strain at this stage. At 2.5–4 min, the coal seam is subjected to stress, extrusion, and pore destruction, its elastic modulus increases, and the strain temporarily stagnates. In the following 4–10 min, the degree of pore damage and rupture of the coal seam gradually increase, the desorption rate of gas molecules accelerates, the gas pressure gradually increases, and the plastic strain of coal seam appears and increases non-linearly. In the next 10 min of unloading, the loading stress is higher than the upper limit of the pressure of the recovery deformation due to the plastic deformation of the coal; therefore, the coal fails to return to the initial state in time. At this time, the strain does not change. Until 6 min of unloading, the coal strain decreases when the stress is 1.009 MPa. The strain decreases sharply in the last 4 min, and the pores of the coal seam are permanently destroyed. After unloading, the coal seam does not return to its initial state, and the strain of the coal seam is 1.08×10^{-3}. By analyzing the relationship between gas pressure and strain in the loading stage of the previous minute. The analysis of the c and d regions in Figure 5F is consistent with the analysis of the a and b regions in Figure 5C. It can be seen that from the 0.3–1 min loading stage, the elastic strain of coal increases linearly under the influence of stress, and the coal is still in the elastic deformation stage.

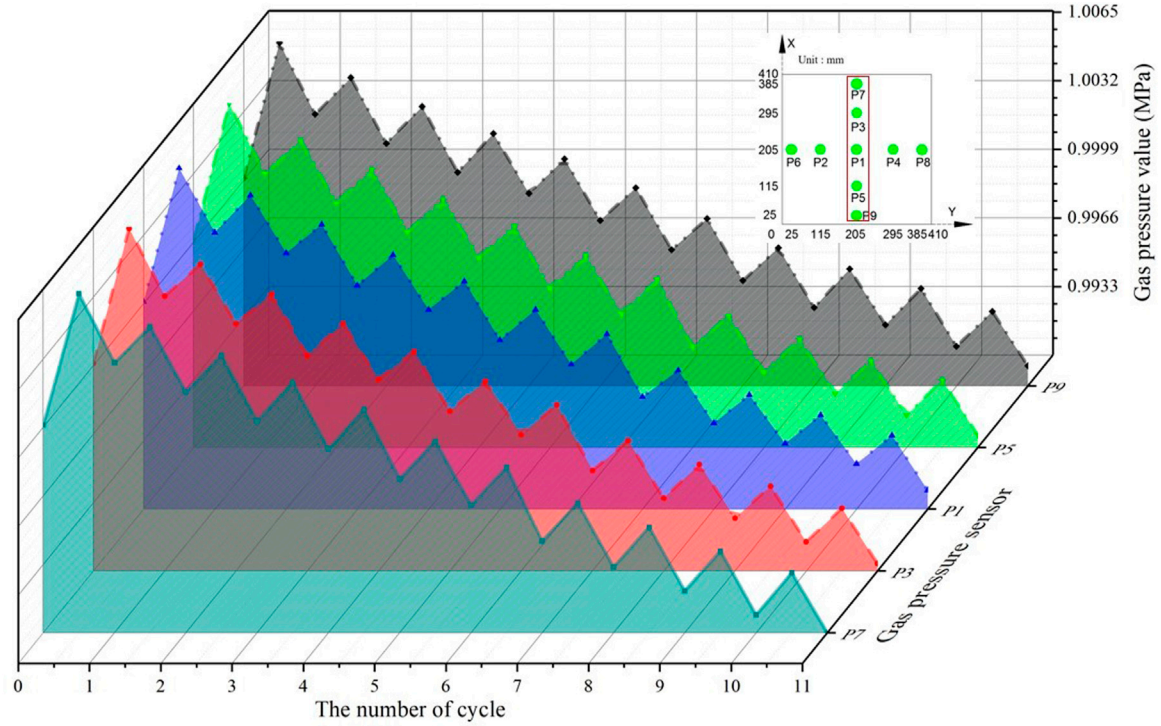

FIGURE 7
Relationship between gas pressure change and cycle number.

According to the correlation equation of coal permeability and strain (Zhu et al., 2019), the strain of coal caused by effective stress and gas adsorption is related to the permeability of coal, and the permeability is also affected by the physical parameters of coal rock such as fracture volume pressure coefficient and coal volume modulus. The calculation formula of coal sample permeability is as follows

$$k = k_0 e^{-3C_f K(\Delta\varepsilon_v + \Delta\varepsilon_s)}. \quad (2)$$

In the formula, k_0 is the initial permeability of coal sample, $10^{-3}\mu m^2$; C_f is the fracture volume compression coefficient, MPa^{-1}; K is the bulk modulus of coal sample; $\Delta\varepsilon_v$ is the volume strain variation of coal sample; the change of $\Delta\varepsilon_s$ is the strain of coal sample caused by the shrinkage of coal matrix caused by the change of gas pressure.

It can be seen from Eq. 2 that the change of coal permeability (k) is mainly affected by the change of coal sample volume strain ($\Delta\varepsilon_v$) and the change of gas pressure, which leads to the shrinkage of coal matrix. Due to the change of gas pressure, the coal strain caused by the shrinkage of coal matrix is very small and can be ignored. Through the strain data of this experiment, it can be concluded that with the increase of the number of cycles, the cumulative damage degree of coal body increases and its permeability gradually decreases. As shown in Figure 6.

Through the analysis of the relationship between stress, strain and gas pressure in the process of cyclic loading and unloading, it is concluded that under the action of mine cyclic mining disturbance stress, the coal body in the loading area is squeezed to produce new cracks, the amount of adsorbed gas gradually increases, and the spatial structure of coal skeleton becomes smaller, and the gas pressure of coal body is increases. Therefore, the risk of gas outburst is the highest, and then the gas migrates from the loading area to the unloading area. This experiment provides a reference for the analysis and prevention of mine gas disasters.

3.2 Evolution characteristics of gas pressure in a coal seam with the number of cyclic disturbances

According to the experimental scheme, the experiment of gas pressure in coal seam with the number of cyclic disturbances is carried out. By analyzing the relationship between the change of sensor gas pressure in the box and the number of cyclic loading and unloading times, the corresponding laws are summarized, so as to discuss the gas migration law in coal body under the action of actual mine disturbance, and better provide reference for the prevention and control of potential safety hazards in actual mining.

Figure 7 shows the sensor gas pressure curve on the first section longitudinal profile with the cycle changes. The gas pressure constantly changes with the cyclic loading and unloading stress and reaches the maximum value after the first loading and unloading (Li et al., 2022a; Li et al., 2022b). At the end of each subsequent loading and unloading, each gas pressure value is smaller than that at the end of the previous loading and unloading. After 11 loading cycles, each gas pressure sensor's pressure value decreases by approximately 0.01 MPa.

Figure 8 shows the relationship between gas pressure changes and different loading and unloading cycles under a

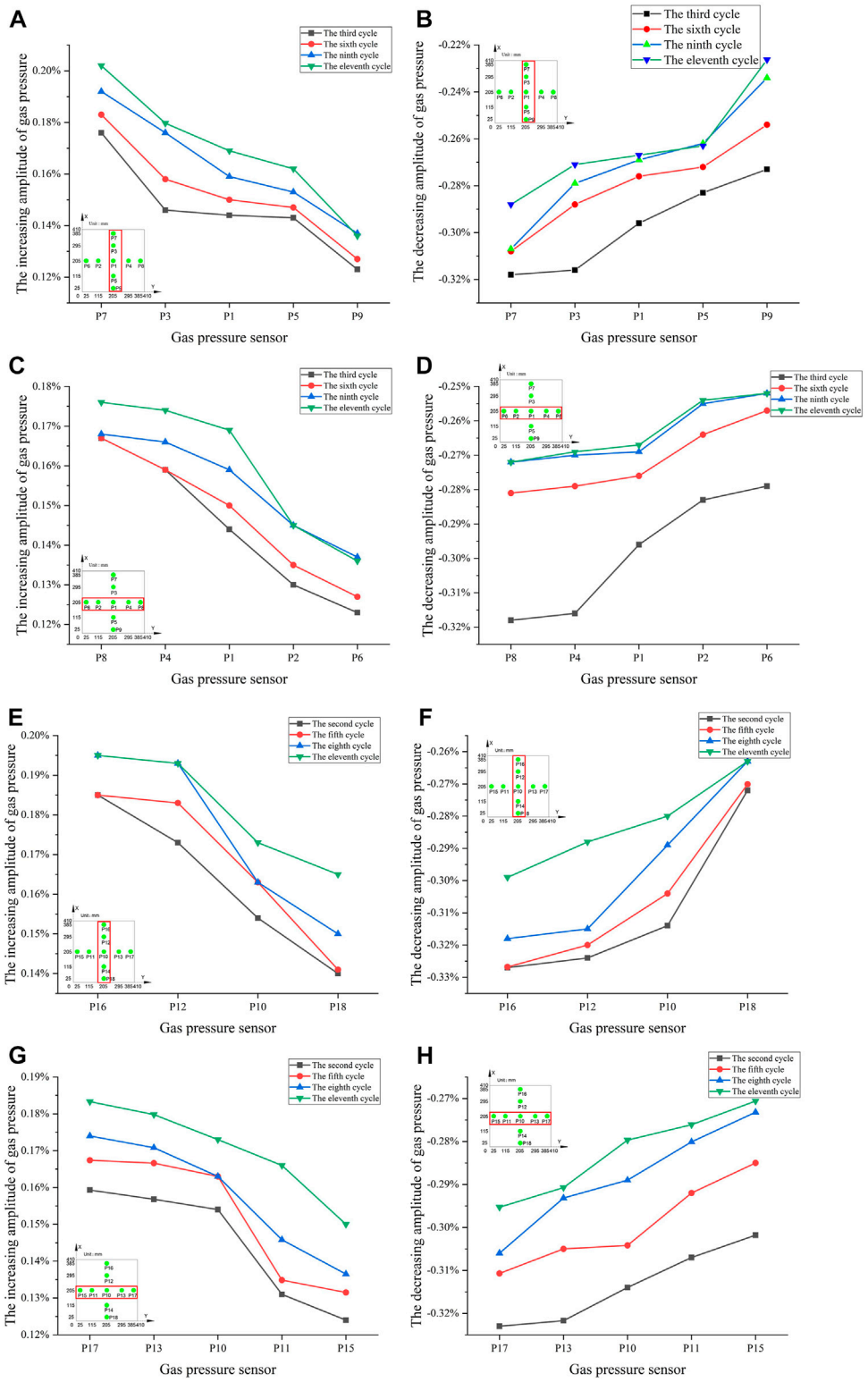

FIGURE 8
Relationship between gas pressure and cycle times.

stable gas pressure of 1.0 MPa. The increase in gas pressure P is obtained by analyzing each gas pressure value V after each loading and gas pressure value W after the end of the previous unloading, and the gas pressure's reduction quantity Q is obtained. The increase and decrease in each sensor pressure P and Q under 11 loading and unloading cycles were analyzed

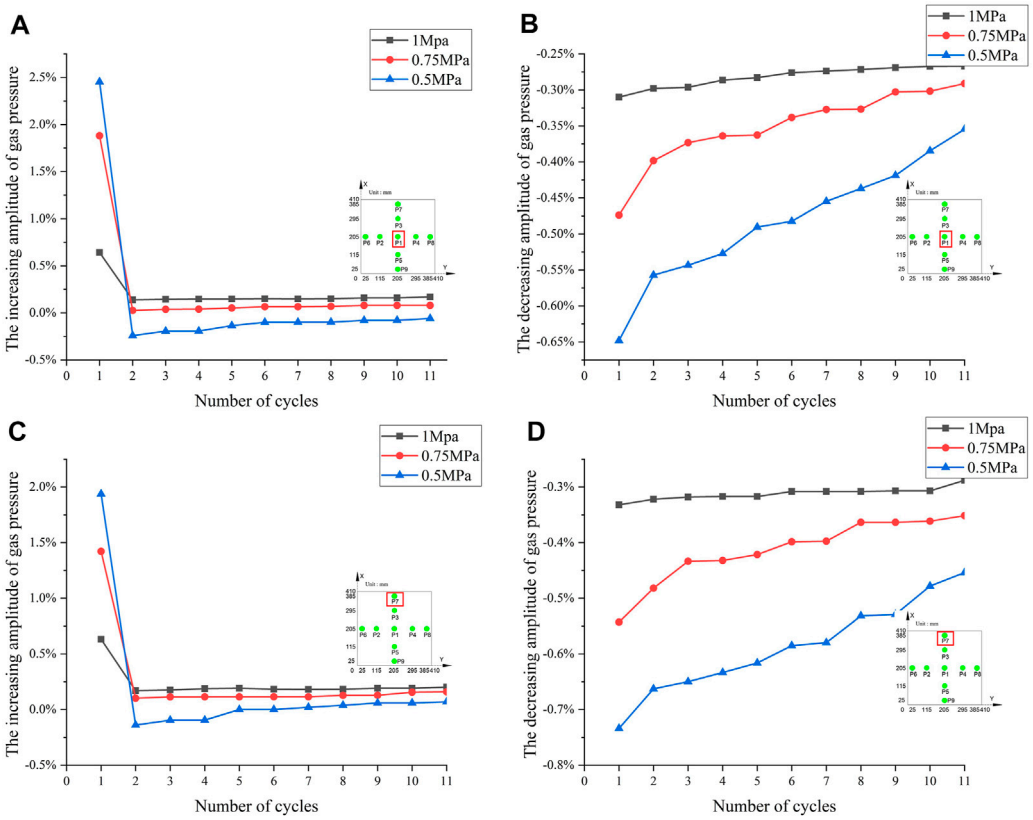

FIGURE 9
The changing law of gas pressure under different initial conditions.

and processed, and the growth and drop of each gas pressure M and N were obtained.

$$M_{z,n} = \frac{V_{z,n} - W_{z,n-1}}{W_{z,n-1}}, \quad (3)$$

$$N_{z,n} = \frac{W_{z,n} - V_{z,n}}{V_{z,n}}, \quad (4)$$

n is the number of cycles (when $n = 1$, Wz, 0 is the gas pressure value before loading). Z is the gas pressure sensor.

The experimental results in Figures 8A–H are obtained through data analysis. Figures 8A, B show the comparison of the increasing amplitude of gas pressure and the decreasing amplitude of gas pressure of the P7, P3, P1, P5, and P9 sensors under the 3rd, 6th, 9th, and 11th cycles of loading and unloading stress, respectively. Taking the P7 sensor as an example, it is concluded that $M_{7,11} > M_{7,9} > M_{7,6} > M_{7,3}$ and $N_{7,11} < N_{7,9} < N_{7,6} < N_{7,3}$. See Figures 8A, B, With the increased cycles, the damage degree of coal after each loading is greater than that after the previous loading, coal deformation causes more gas to be squeezed out, increasing the increasing amplitude of gas pressure accordingly. After each unloading, the increment of coal strain gradually decreases and stabilizes, and the number of new cracks gradually decreases. The number of gas molecules adsorbed into new coal cracks decreases correspondingly during unloading, and the decreasing amplitude of gas pressure reduces. Therefore, it is concluded that as the number of cycles increases, the increasing amplitude of gas pressure gradually increases, and the decreasing amplitude of gas pressure gradually decreases. The gas increasing and decreasing amplitude of P3, P1, P5 and P9 sensors also have the above rules.

Taking the third cycle loading and unloading process as an example, it is concluded that $M_{7,3} > M_{3,3} > M_{1,3} > M_{5,3} > M_{9,3}$ and $N_{7,3} > N_{3,3} > N_{1,3} > N_{5,3} > N_{9,3}$. See Figures 8A, B, The P7 sensor is closest to the loading and unloading pressure head, and the damage degree of coal seam under the action of stress is more obvious, causing more new cracks than other sensor positions, resulting in the largest increasing amplitude of gas pressure during loading. The farther the coal seam is from the pressure head, the smaller the impact on and increasing amplitude of gas pressure. During unloading, the closer the distance is to the loading and unloading pressure head, the more gas molecules are adsorbed into the cracks of the coal seam, leading to the biggest decreasing amplitude of gas pressure. The farther away from the loading and unloading pressure head, the less affected the coal seam is and the smaller the decreasing amplitude of gas pressure. According to the analysis, the 6th, 9th, and 11th loading and unloading conform to the law and apply to several other sections.

Through the above analysis, it is concluded that the increasing amplitude of gas pressure increases with the increase of the number of cycles during loading, and the closer to the pressure head area, the greater the increasing amplitude of gas pressure; during unloading, the decreasing amplitude of gas pressure decreases with the increase of cycle times, and the closer to the indenter region, the greater the

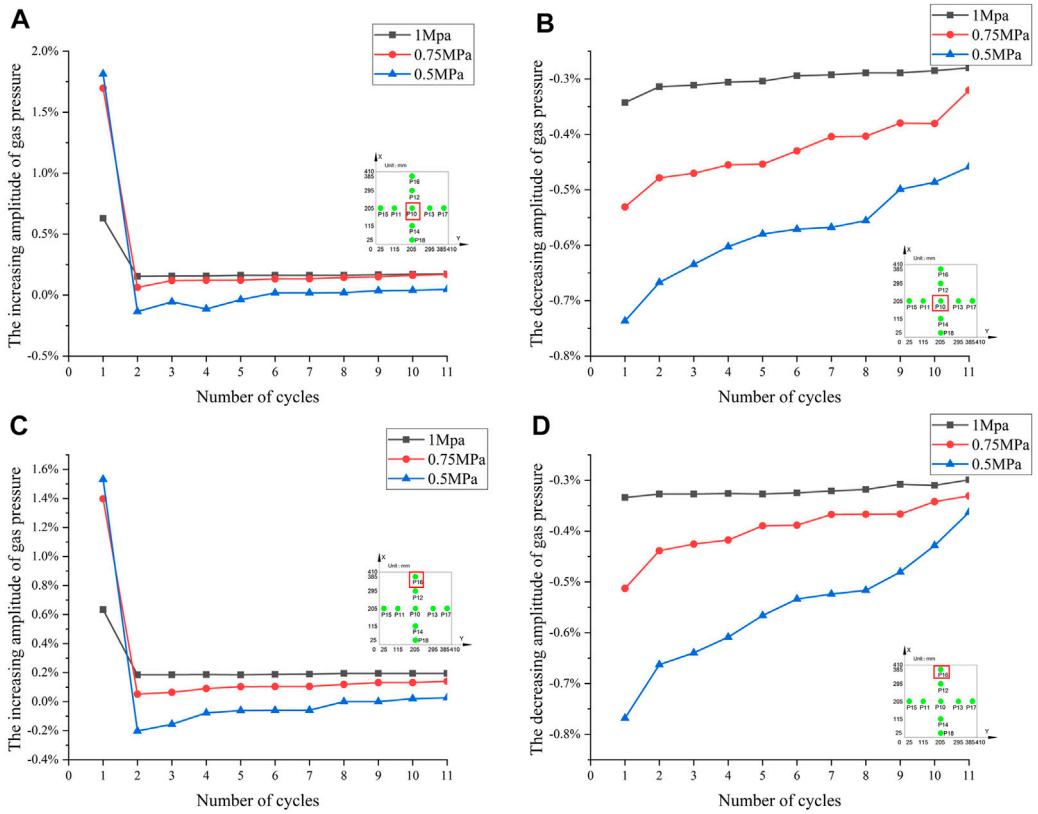

FIGURE 10
The changing law of gas pressure under different initial conditions.

decreasing amplitude of gas pressure. This law can provide reference for the prediction and analysis of coal seam gas pressure in front of the actual mine circular coal mining work, and reduce the risk of gas outburst.

3.3 The changing law of gas pressure under different initial conditions

Due to geographical location, climatic conditions, coal deterioration, porosity, *etc.*, the actual distribution of gas pressure in mining face is different. Therefore, experimental studies were conducted for different initial gas pressure conditions in coal mines, and the following research results were obtained.

Figure 9 shows the curves of gas pressure and number of cycles at different initial gas pressures in the first section. Since the adsorbed gas of the coal seam has reached the saturated state before loading, under the initial gas pressure of 1 MPa, the gas in the cracks of the coal seam is squeezed out through the loading stress, resulting in the increase of the gas pressure of the position sensor and the largest increasing amplitude of gas pressure. Under the initial gas pressure of 0.75 MPa, due to the small initial gas pressure, the effective stress of the loading stress is larger than that of the initial gas of 1 MPa. The degree of damage to the coal body is relatively high, and more new cracks are generated. The coal body adsorbs more gas, resulting in a smaller increase in gas pressure. Under the initial gas pressure of 0.5 MPa, the effective stress of coal seam is the largest and the degree of coal fracture is the highest. The amount of gas absorbed by the new fracture of coal seam is greater than the amount of gas overflowed by extrusion. Resulting in a negative increase in the gas pressure of the sensor, and in the loading, the initial gas pressure of 0.5 MPa coal gas adsorption is greater than the initial gas pressure of 0.75 MPa coal gas adsorption, as shown in Figures 9A, C. It is concluded that the greater the initial gas pressure value, the greater the increasing amplitude of gas pressure in the same cycle.

Through data analysis: the smaller the initial gas pressure is, the higher the degree of fracture of the coal body under the action of circulation is. In the unloading stage, more free gas diffuses into the new fracture, resulting in the maximum decreasing amplitude of the gas with the initial gas of 0.5 MPa, followed by the initial gas pressure of 0.75 MPa, and the decreasing amplitude of the initial gas pressure of 1 MPa is the smallest. It is concluded that the greater the initial gas pressure value, the smaller the decreasing amplitude of gas pressure in each cycle. As shown in Figures 9B, D. The image described in Figures 10A–D still conforms to the above analysis.

By exploring the change law of coal gas with cyclic loads under varying initial gas pressures, the above gas pressure change characteristics are obtained, providing data support and reference for analyzing the risk and prevention of gas outbursts in the working

face caused by cyclic mining times and different initial gas pressures in actual cyclic mining.

4 Conclusion

(1) The influence of stress loading and unloading on the gas pressure of raw coal is different. The gas pressure increases during loading and decreases during unloading. Gas pressure is affected by both stress and damage accumulation. As the number of cycles increases, the damage of raw coal increases, and the newly generated cracks adsorb more free gas molecules, resulting in a decrease in the gas pressure in raw coal.

(2) The increasing and decreasing amplitude of gas pressure in raw coal are closely related to cycle number and specific location. The closer to the pressure shaft area during loading, the greater the increasing amplitude of gas pressure, and the closer to the pressure shaft area during unloading, the smaller the decreasing amplitude of gas pressure; at the same position, the increasing amplitude of gas pressure increases with the increase of cycle times, and the decreasing amplitude of gas pressure decreases with the increase of cycle times.

(3) Different initial gas pressure in raw coal shows different physical properties. Under 0.5 MPa gas pressure, due to the small internal pressure of the box, the cumulative damage of the coal body caused by cyclic loading is more serious than that under 0.75 and 1 MPa gas pressure, and the internal pressure of the box always decreases. When loading, the increasing amplitude of gas pressure at the initial gas pressure of 1 MPa is more significant than that at 0.5 and 0.75 MPa. The greater the initial gas pressure during unloading, the smaller the decreasing amplitude of gas pressure. It shows that the damage of coal body is affected by the gas pressure of coal body. The smaller the gas pressure, the easier the coal body is destroyed, and the coal matrix and new cracks can adsorb more gas molecules.

Data availability statement

The original contributions presented in the study are included in the article/Supplementary Material, further inquiries can be directed to the corresponding author.

Author contributions

JG designed the test protocol, carried out experimental operations, collected experimental data, and established the final draft. JL analyzed the experimental data, wrote the first draft and participated in the entire process of writing the article. GZ participates in the drawing of the picture. DZ and ZX make comments and suggestions on the article. JX conducted the experimental operation and fully supervised the entire paper.

Funding

This work was supported by National Natural Science Foundation of China (No. 52064016); China Postdoctoral Science Foundation Funded Project (2022M722924); Jiangxi Science and Jiangxi Provincial Tousand Talents Plan Project (jxsq2019102082) and National Natural Science Foundation of China (No.52264018).

Conflict of interest

Author JG was employed by Sinosteel MaanShan General Institute of Mining Research Co. Ltd.

The remaining authors declare that the research was conducted in the absence of any commercial or financial relationships that could be construed as a potential conflict of interest.

Publisher's note

Supplementary material

The Supplementary Material for this article can be found online at: https://www.frontiersin.org/articles/10.3389/feart.2023.1080472/full#supplementary-material

References

Chen, Y., Zuo, J. P., Song, H. Q., Feng, L. L., and Shao, G. Y. (2018). Deformation and crack evolution of coal-rock combined body under cyclic loading-unloading effects. *J. Min. Saf. Eng.* 35 (4), 0826–0833.

Cheng, Q. Y., Li, B. B., Li, J. H., Gao, Z., and Wang, B. (2021). Coal fracture's compressibility and permeability under proppant embedding. *China Saf. Sci. J.* 31 (10), 105–111.

Duo, Y. Y., Sun, L. L., Wang, P. F., and Feng, R. X. (2018). Research and application of stress-seepage relationship of coal in heading face of liangbaosi coal mine under true triaxial test. *Min. Saf. Environ. Prot.* 45 (2), 0001–0005.

Gao, K., Qiao, G. D., Liu, Z. G., Liu, J., Zhu, F. H., Zhang, S. C., et al. (2019). On classification conception of coal and gas outburst mechanism and its application. *J. Min. Saf. Eng.* 36 (5), 1043–1051.

Geng, J. B., Xu, J., Nie, W., Peng, S. J., Zhang, C. L., and Luo, X. H. (2017). Regression analysis of major parameters affecting the intensity of coal and gas outbursts in laboratory. *Int. J. Min. Sci. Technol.* 27 (2), 327–332. doi:10.1016/j.ijmst.2017.01.004

He, J., Okere, C. J., Su, G., Hu, P., Zhang, L., Xiong, W., et al. (2021). Formation damage mitigation mechanism for coalbed methane wells via refracturing with fuzzy-ball fluid as temporary blocking agents. *J. Nat. Gas Sci. Eng.* 90, 103956. doi:10.1016/j.jngse.2021.103956

Hu, G., Zhao, Q. H., He, Y. S., and Han, G. (2016). Elastic modulus's evolution law of plagiogranite under cyclic loading. *J. Eng. Geol.* 24 (5), 0881–0890.

Jia, H. Y., Wang, K., Wang, Y. B., and Sun, X. K. (2018). Permeability characteristics of gas-bearing coal specimens under cyclic loading-unloading of confining pressure. *J. China Coal Soc.* 45 (5), 1710–1714.

Li, Q. H., Song, D. Q., Yuan, C. M., and Nie, W. (2022). An image recognition method for the deformation area of open-pit rock slopes under variable rainfall. *Measurement* 188, 110544. doi:10.1016/j.measurement.2021.110544

Li, Q. M., Liang, Y. P., and Zou, Q. L. (2019). Seepage and damage evolution characteristics of different gas-bearing coal under cyclic loading-unloading conditions. *J. China Coal Soc.* 44 (09), 2803–2815.

Li, X. P., Wang, B., and Zhou, G. L. (2012). Research on distribution rule of geostress in deep stratum in Chinese mainland. *J. Rock Mech. Eng.* A1, 2875–2880.

Li, X. S., Li, Q. H., Hu, Y. J., Chen, Q., Peng, J., Xie, Y., et al. (2022). Study on three-dimensional dynamic stability of open-pit high slope under blasting vibration. *Lithosphere* 2021, 2022. doi:10.2113/2022/6426550

Li, X. S., Li, Q. H., Hu, Y. J., Teng, L., and Yang, S. (2021). Evolution characteristics of mining fissures in overlying strata of stope after converting from open-pit to underground. *Arabian J. Geosciences* 14 (24), 1–18. doi:10.1007/s12517-021-08978-0

Lin, B. Q., Yan, F. Z., Zhu, C. J., Zhou, Y., Zou, Q., Guo, C., et al. (2015). Cross-borehole hydraulic slotting technique for preventing and controlling coal and gas outbursts during coal roadway excavation. *J. Nat. Gas Sci. Eng.* 26, 518–525. doi:10.1016/j.jngse.2015.06.035

Liu, D., Xu, J., Yin, G. Z., Wang, W. Z., Liang, Y. Q., and Peng, S. J. (2013). Development and application of multifield coupling testing system for dynamic disaster in coal mine. *J. Rock Mech. Eng.* 32 (05), 0966–0975.

Liu, D., Xu, J., Yin, G. Z., Wang, W. Z., Liang, Y. Q., and Peng, S. J. (2013). Development and application of multifield coupling testing system for dynamic disaster in coal mine. *Chin. J. Rock Mech. Eng.* 32 (5), 0966–0975.

Liu, H., Su, G., Okere, C. J., Li, G., Wang, X., Cai, Y., et al. (2022). Working fluid-induced formation damage evaluation for commingled production of multi-layer natural gas reservoirs with flow rate method. *Energy* 239, 122107. doi:10.1016/j.energy.2021.122107

Liu, Z. Y., Wang, G., Cheng, W. M., Qin, X. J., and Han, D. Y. (2020). Experimental study on seepage characteristics of coal under truly triaxial loading and unloading based on different minimum principal stress properties. *Earth Environ. Sci.* 570, 042039. doi:10.1088/1755-1315/570/4/042039

Lu, Y. Y., Peng, Z. Y., Xia, B. W., Yu, P., and Ou, C. N. (2020). Coal and gas multi-functional physical model testing system of deep coal Petrography engineering. *J. China Coal Soc.* 45 (S1), 272–283.

Nie, B. S., Ma, Y. T., He, X. Q., and ZhaoLiu, D. X. F. (2022). Formation and propagation law of coal and gas outburst impact airflow. *J. China Coal Soc.* 47 (1), 333–347.

Nie, B. S., Ma, Y. T., He, X. Q., and ZhaoLiu, D. X. F. (2022). Micro-scale mechanism of coal and gas outburst: A preliminary study. *J. China Univ. Min. Technol.* 51 (2), 207–220.

Pan, Y. S. (2016). Integrated study on compound dynamic disaster of coal-gas outburst and rockburst. *J. China Coal Soc.* 41 (1), 105–112.

Ren, S., Wang, Z. X., and Zhang, C. (2021). Experimental study on permeability characteristics of coal under different confining pressure and air pressure. *Min. Res. Dev.* 41 (1), 0100–0105.

Sun, G. Z., Xu, X., Tian, K. Y., and Zhang, R. L. (2016). Experimental research on response characteristics of permeability of coal containing gas on axial cycle loading. *J. Geophys. Eng.* 47 (06), 29–32.

Tao, X., Okere, C. J., Su, G., and Zheng, L. (2022). Experimental and theoretical evaluation of interlayer interference in multi-layer commingled gas production of tight gas reservoirs. *J. Petroleum Sci. Eng.* 208, 109731. doi:10.1016/j.petrol.2021.109731

Wang, D. K., Yu, C., Wei, J. P., Wei, Q., and Fu, J. H. (2020). Seepage characteristics of loaded fractured coal based on LBM Method. *Chin. J. Rock Mech. Eng.* 39 (4), 0695–0704.

Wang, E. Y., Zhang, G. R., Zhang, C. L., and Li, Z. H. (2022). Research progress and prospect on theory and technology for coal and Gas outburst control and protection in China. *J. China Coal Soc.* 47 (1), 287–322.

Wang, H. P., Li, Q. C., Yuan, L., Li, S., Xue, J., Zhu, H., et al. (2018). Similar material research and property analysis of coal bunker in coal and gas out-burst simulation test. *J. China Univ. Min. Technol.* 35 (6), 1277–1283.

Wang, X. L., Geng, J. B., Zhang, D. M., Xiao, W. J., Chen, Y., and Zhang, H. (2022). Influence of sub-supercritical CO2 on pore structure and fractal characteristics of anthracite: An experimental study. *Energy* 261, 125115. doi:10.1016/j.energy.2022.125115

Wang, X. Y., Zhou, H. W., Zhong, J. C., Zhang, L., Wang, C. S., and An, L. (2018). Study on energy evolution and permeability characteristics of deep coal damage under triaxial cyclic loading and unloading conditions. *Chin. J. Rock Mech. Eng.* 37 (12), 2676–2784.

Xie, H. P., Zhou, H. W., Liu, J. F., Gao, F., Zhang, R., Xie, J. D., et al. (2011). Mining-induced mechanical behavior in coal seams under different mining layouts. *J. China Coal Soc.* 36 (7), 1607–1074.

Xu, J., Geng, J. B., Peng, S. J., Yuan, M., Zhang, C. L., Luo, X. H., et al. (2018). Analysis of the pulsating development process of coal and gas outburst. *J. China Univ. Min. Technol.* 47 (1), 145–154.

Xu, J., Li, B. B., Zhou, T., Cao, J., and Ye, G. B. (2014). Experimental study of deformation and seepage characteristics of coal under cyclic loading. *Chin. J. Rock Mech. Eng.* 33 (2), 0225–0234.

Yan, F. Z., Lin, B. Q., Zhu, C. J., Shen, C., Zou, Q. L., Guo, C., et al. (2015). A novel ECBM extraction technology based on the integration of hydraulic slotting and hydraulic fracturing. *J. Nat. Gas Sci. Eng.* 22, 571–579. doi:10.1016/j.jngse.2015.01.008

Yang, X. B., Chen, H. M., Lv, J. Q., Hou, X., and Nie, C. G. (2019). Energy consumption ratio evolution law of sandstones under triaxial cyclic loading. *Rock Soil Mech.* 40 (10), 3751–3758.

Yao, J., Zhu, P., Guo, L., Duan, L., Zhang, Z., Kurko, S., et al. (2022). Commentary on "A continuous hydrogen absorption/desorption model for metal hydride reactor coupled with PCM as heat management and its application in the fuel cell power system. *Int. J. Hydrogen Energy* 47 (19), 10799–10801. [Yao J, Zhu P, Guo L, Duan L, Zhang Z, Kurko S et al. Int J Hydrogen Energy 2020. https://doi.org/10.1016/j.ijhydene.2020.05.089]. doi:10.1016/j.ijhydene.2021.12.231

Zhang, X., Li, B. B., Ren, C. H., Xu, J., and Li, J. H. (2020). Energy mechanism analysis on elastoplastic damage of coal under cyclic loading. *China Saf. Sci. J.* 30 (05), 88–94.

Zhang, Y., Okere, C. J., and Su, G. (2021). Effect of loading rates on accurate *in-situ* stress determination in different lithologies via Kaiser effect. *Arabian J. Geosciences* 14 (14), 1–8. doi:10.1007/s12517-021-07674-3

Zhao, J., Guo, G. T., Xu, D. P., Huang, X., Hu, C., Xia, Y. L., et al. (2020). Experimental study of deformation and failure characteristics of deeply-buried hard rock under triaxial and cyclic loading and unloading stress paths. *Rock Soil Mech.* 41 (5), 1521–1530.

Zhao, J., Guo, G. T., Xu, D. P., Huang, X., Hu, C., Xia, Y. L., et al. (2020). Experimental study of deformation and failure characteristics of deeply-buried hard rock under triaxial and cyclic loading and unloading stress paths. *Rock Soil Mech.* 41 (5), 1521–1530.

Zhou, S. N., and He, X. Q. (1990). Coal and gas multi-functional physical model testing system of deep coal Petrography engineering. *J. China Univ. Min. Technol.* 19 (2), 1–8.

Zhu, J., Tang, J., Wang, Q., Lan, T., and Jiang, Y. (2019). Correlation between permeability and strain of coal samples under loading. *J. China Coal Soc.* 44 (S2), 566–573.

Zou, J. K., Chen, W. Z., Yang, D. S., Yuan, J. Q., and Tian, X. J. (2016). Mechanical properties and damage evolution of coal under cyclic loading conditions. *J. China Coal Soc.* 41 (7), 1675–1682.